# Dynamics of "Hot" Oxygen Atoms on Ag (100) Surface upon O<sub>2</sub> Dissociation

Kaixuan Gu,<sup>1,2</sup> Sen Lin,<sup>1,\*</sup> and Hua Guo,<sup>2,\*</sup>

<sup>1</sup>State Key Laboratory of Photocatalysis on Energy and Environment, College of

Chemistry, Fuzhou University, Fuzhou 350002, China

<sup>2</sup>Department of Chemistry and Chemical Biology, University of New Mexico,

Albuquerque, New Mexico, 87131, USA

<sup>\*</sup>Corresponding authors. Emails: <a href="mailto:slin@fzu.edu.cn">slin@fzu.edu.cn</a> (S.L) and <a href="mailto:hguo@unm.edu">hguo@unm.edu</a> (H.G.)

#### **Abstract**

The dynamics of ballistic adsorbates on metal surfaces are not only important for understanding energy dissipation, but also of practical relevance in an array of important applications including corrosion and heterogeneous catalysis. In this work, we examine the early dynamics of "hot" O atoms produced by dissociative chemisorption of O<sub>2</sub> on a Ag(100) surface, taking advantage of a high-fidelity machine learned high-dimensional potential energy surface based on first-principles data. Our classical trajectory simulations revealed that the experimentally observed large O-O separations (2-4 nm) can only be reached with hyperthermal incident O<sub>2</sub>. With thermally impinging O<sub>2</sub>, the calculated separation between the equilibrated O atoms is about one order of magnitude shorter (~ 0.3 nm). The relatively low mobility of the "hot" O atoms on this surface is attributed to the fast energy dissipation to surface phonons and a relatively high diffusion barrier. In addition, the O atom diffusion exhibits strong anisotropy dictated by the potential energy surface.

# I. Introduction

Reactions on heterogeneous catalyst surfaces are often initiated by adsorption and/or dissociation of gas phase molecules. Such processes are mostly exothermic, which may lead to a substantial energy release. While energy dissipation to the corrugated substrate is typically fast, there is evidence suggesting that thermalization might take a sufficiently long time for translationally "hot" adsorbates to exhibit transient mobility on the surface. In some cases, they might even initiate reactions with co-adsorbates. Importantly, the dynamics of such ballistic or translationally "hot" atoms and molecules reveal valuable information about the rate of energy dissipation to the surface, which have attracted much recent attention, both experimentally and theoretically. In addition, the existence of such "hot" precursors is in sharp contrast to the conventional depiction of kinetics of surface reactions within a Markovian hopping framework. A better understanding of such processes is thus fundamentally important for the development of predictive models for heterogeneous catalysis. A support of the development of predictive models for heterogeneous catalysis.

Oxidation of metals by oxygen molecules is of key interest in various practical applications and extensively studied in surface science.<sup>24</sup> The dissociation of O<sub>2</sub> on various metal surfaces is known to be highly exothermic,<sup>25</sup> producing energetic O atoms at the surface.<sup>2</sup> Experimental identification and characterization of "hot" fragments are often challenging due to their high reactivity and short lifetime. Scanning Tunneling Microscopy (STM) has been used to measure the separation of O atom pairs on various metal surfaces formed from O<sub>2</sub> dissociation, which are attributed to the "hot" O atom motion.<sup>26-35</sup> These measurements were typically performed at low temperatures in order to suppress thermal diffusion. However, there are significant controversies concerning the STM extracted information. For example, the initial report by Brune et al.<sup>26,27</sup> that "hot" O atoms reach separations at least 8 nm on an Al(111) surface, which correspond to 28 surface lattice constants (SLCs), was later challenged by Schmid et al.,<sup>32</sup> whose STM results indicated that the O-O pairs are separated by only ~1-2 SLCs, namely ~0.25 - 0.5 nm.

The aforementioned STM experiments have stimulated many theoretical studies. 14, 16, 21, 36-42 For example, the earlier theoretical simulation of Wahnström et al. on the "hot" O dynamics on Al(111) suggested a relatively short O-O separation, <sup>36</sup> supporting the experiment of Schmid et al.<sup>32</sup> However, this pioneering study used an empirical potential energy surface (PES) that might not be quantitatively accurate. More recent efforts have endeavored to take advantage of first-principles description of the PES. 14, 16, 21, 37-42 Besides the accuracy of the PES, an reliable simulation of the "hot" atom dynamics is also challenging because the energy exchange with surface phonons, and sometimes surface electron-hole pairs, needs be characterized faithfully. This necessarily requires a large supercell that is capable of describing the phonon spectrum. To tackle this problem, Meyer and Reuter proposed a Me/QM model, in which a relatively small region of the surface described by quantum mechanical (QM) method is embedded in the metal (Me) described by a force field. 14 Despite its success in gaining insights into the dynamics, 16, 41 this method still requires Ab Initio Molecular Dynamics (AIMD) calculations in the QM region, which are computationally intensive.

In this work, we examine the dynamics of "hot" O atoms upon dissociation of O<sub>2</sub> on a Ag(100) surface, which has been investigated experimentally by Morgenstern and coworkers by depositing O<sub>2</sub> molecules on such a surface at low surface temperatures (140 or 200 K).<sup>31, 34</sup> The STM measured O-O pair distance distribution shows two peaks near 2 and 4 nm, corresponding to 7 and 14 SLCs (0.29 nm for Ag(100)). Another STM study from the same group initiated the O<sub>2</sub> dissociation through inelastic electron tunneling and found two peaks at 1 and 2 nm.<sup>43</sup> Such distances are much less than the 8 nm reported by Brune et al.,<sup>26, 27</sup> but still larger than other STM studies of O<sub>2</sub> dissociation on metal surfaces,<sup>28-30, 32, 33, 35</sup> which are typically close to or less than 1 nm. These authors attributed the large O-O separations to strong repulsion between adsorbed O atoms. So far, no simulations have been reported on this system to explain these observations. Our approach used in this work differs from the Me/QM method in that the surface is modeled using a machine-learned high-dimensional PES,<sup>44, 45</sup> which has the same accuracy as the first-

principles density functional theory (DFT), but much less computationally intensive. As a result, we can afford to use a large supercell and perform long-time simulations, as demonstrated in our recent studies on "hot" H and N atom diffusion dynamics on metal surfaces.<sup>21, 46</sup> A similar approach has recently been adapted by Lin and Jiang, who extensively investigated the post-dissociation dynamics for O<sub>2</sub> on Pd surfaces.<sup>42</sup>

# II. Methods

All spin-polarized DFT calculations were carried out using the Vienna Ab initio Simulation Package (VASP).<sup>47, 48</sup> The Kohn-Sham orbitals of the valence electrons were represented with a plane wave basis with a cutoff energy of 380 eV and the core electrons were approximated by the projector augmented wave approach.<sup>49</sup> Several GGA (generalized gradient approximation) functionals were tested and the revised Perdew-Burke-Ernzerhof (RPBE) functional<sup>50</sup> was employed to describe the electron exchange-correlation, as the diffusion barrier for O is not sensitive to the choice of the functional, as shown in Table S1 in Supporting Information (SI). For static calculations, a Ag(100) slab with  $3 \times 3$  supercell and four atomic layers was constructed. In order to construct a PES suitable for different supercell sizes, a larger Ag(100) slab was modeled by 8 atomic layers and a  $5 \times 5$  supercell. A  $4 \times 4 \times 1$  kpoint grid and a  $\Gamma$ -point grid were used to characterize the Brillouin zones of the (3  $\times$ 3) and  $(5 \times 5)$  Ag(100) models, respectively. All atoms except those in the bottom surface layer were allowed to move. The slabs were separated by a vacuum space of 16 Å in the Z direction. The energy barriers were calculated employing the climbing image nudged elastic band (CI-NEB) method from the VTST tools,<sup>51</sup> with the force convergence criterion of 0.05 eV/Å. The adsorption energy is computed as the energy difference between the adsorbed and the surface + gas systems.

The  $O_2$  + Ag(100) PES appropriate for various supercell sizes was constructed by the Embedded Atom Neural Network (EANN) approach.<sup>52</sup> This is an atomistic NN approach,<sup>53</sup> in which the interaction energy is expressed as a sum of atomic contributions, which are controlled by the surroundings. Two hidden layers with 20

and 40 neurons and a cut-off radius of 6 Å were used in the EANN fitting. An uncertainty-driven active learning strategy<sup>54, 55</sup> was adopted to sample data points, which does not need running trajectories to explore the configuration space. The PES was fitted using 3810 DFT points, comprising 1680 points from the  $(3 \times 3)$ -4 layer Ag(100) slab and 2130 points from the  $(5 \times 5)$ -8 layer Ag(100) slab. These training data include both energies and gradients. 90% of the total 3810 points were used for training and the rest for testing. Thanks to the atomic centered nature of EANN, the PES can be used to represent the  $O_2 + Ag(100)$  system with arbitrary supercell sizes larger than or equal to the  $(3 \times 3)$ -4 layer model. It also possesses permutation invariance with respect to the exchange of identical atoms.

In the quasi-classical trajectory (QCT) calculations, the "hot" O atoms were prepared in two ways. At high incidence energies, the  $O_2$  molecule was initially placed at 6.0 Å above the surface. The initial polar and azimuthal angles of the impinging  $O_2$  were randomly sampled. Several different initial conditions were considered, including the incidence polar angle ( $\theta_i$ ), the incidence energy ( $E_i$ ), and the vibrational and rotational quantum numbers ( $v_i$  and  $j_i$ ). At low incidence energies, however, the dissociation probability was so small that the above strategy became statistically impracticable. Under such circumstances, the  $O_2$  moiety was placed at the dissociation transition state and a small kinetic energy was randomly assigned to both O atoms with opposite directions. In all calculations, the surface temperature was set to the experimental value of 140 K.<sup>31</sup> The trajectories were propagated using a modified VENUS code <sup>57</sup> for 2.2 ps with a time step of 0.10 fs.

# III. Results and Discussion

### **IIIA. DFT calculations**

The adsorption sites of the  $O_2$  molecule on the Ag(001) surface were determined based on DFT calculations using the 3 × 3 supercell. The most stable configuration for  $O_2$  is at the 4-fold hollow site with an adsorption energy of 1.10 eV. The  $O_2$  adsorbate lies parallel to the surface with the two oxygen atoms pointing towards nearby bridge

sites and the O-O bond length of 0.143 nm is elongated from the equilibrium geometry of the isolated molecule (0.124 nm). Another adsorption site is the bridge site with an adsorption energy of 0.75 eV, in which the O-O bond length is 0.135 nm. The top views of the two configurations are shown in Figure 1. The results are consistent with previous DFT calculations.<sup>58</sup> Experimentally, a HREELS study found two different adsorption sites of the oxygen molecules with slightly shifted vibrational frequencies at 79 and 84 meV.<sup>59</sup> The adsorption energy of  $O_2$  was measured to be  $\sim$ 0.8 eV.<sup>60</sup> Our DFT results are consistent with these experimental findings.

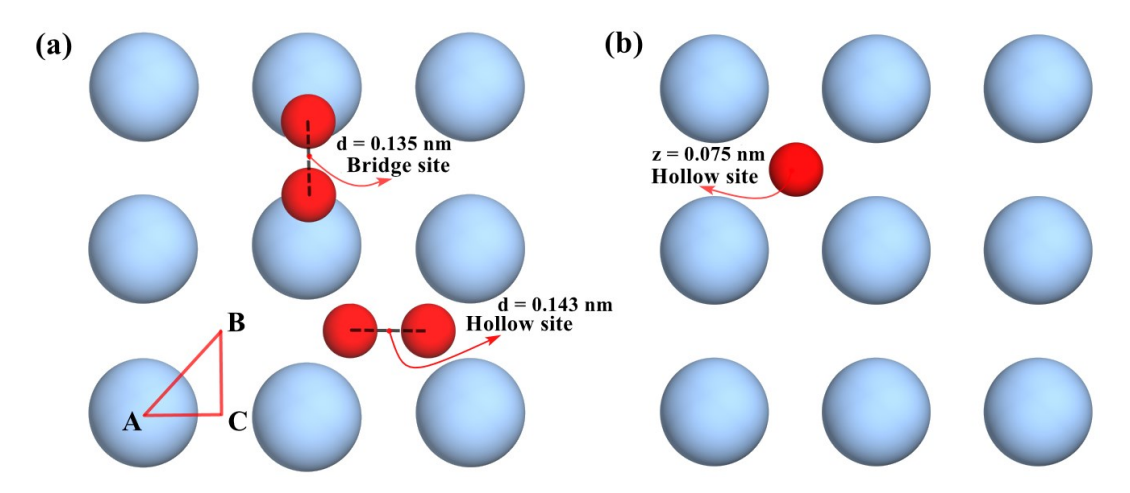
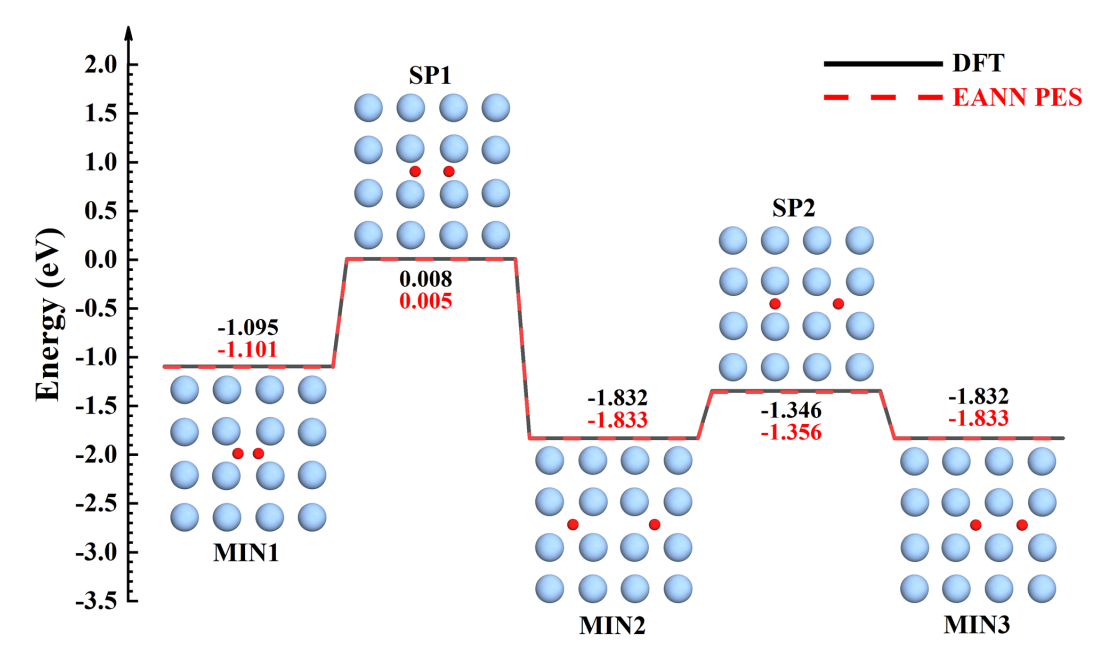


Figure 1. Adsorption sites of the  $O_2$  molecule (a) and O atom (b) on the Ag(100) surface with a (3×3) supercell. The impact region for the scattering calculations is indicated by the reduced triangle ABC. Red and light blue spheres represent O and Ag atoms, respectively. For clarity, only the top layer of the Ag(100) surface is shown.

A saddle point (SP1) for dissociation was found at the hollow site. From the hollow adsorption site (MIN1), the transition state features an elongated O-O bond (0.237 nm) with two O atoms approaching the adjacent bridge sites, as shown in Figure 2. The calculated barrier for O<sub>2</sub> dissociation the Ag(100) surface is 1.10 eV measured from the adsorption well, which is in good agreement with previous theoretical calculations (~1.05 eV).<sup>61</sup> In the final state of the dissociation step (MIN2), the two O atoms occupy two adjacent hollow sites. The energy released from SP1 to

MIN2 is 1.83 eV that is responsible for the formation of two 'hot' O atoms, as discussed below.

The preferred atomic oxygen adsorption site on Ag(100) with the  $3\times3$  supercell is the 4-fold hollow site, as shown in Figure 1, with Z=0.075 nm and an adsorption energy of 3.81 eV, related to the gas phase O( $^3$ P). This result is also consistent with previous DFT reports. The diffusion barrier for a single O atom from one hollow site to an adjacent hollow site via a bridge site is 0.68 eV within the  $3\times3$  model. However, the diffusion barrier (SP2) for an O atom from the MIN2 minimum to MIN3 minimum is only 0.49 eV. The reduction of the diffusion barrier in the presence of another O atom suggests that there is a non-negligible repulsion between two coadsorbed O atoms in the adjacent hollow sites.



**Figure 2.** Energy profiles for O<sub>2</sub> dissociation and O atom diffusion on the (3×3) Ag(100) surface calculated by DFT and by EANN PES. Stable adsorption states for the O<sub>2</sub> molecule and O atoms denoted by potential minima (MIN) and the saddle points (SP) between the minima are presented. Note that MIN2 and MIN3 are identical within the 3×3 model. Red and light blue spheres represent O and Ag atoms, respectively. For clarity, only the top layer of the Ag(100) surface is shown.

#### **IIIB. Accuracy of PES**

The root-mean-square error (RMSE) for the training/validation set is 24.7/30.5 meV in energy per cell and 23.6/29.8 meV/Å in atomic forces. The energy profile of the O<sub>2</sub> dissociation and O diffusion on the (3 × 3) Ag(100) surface on the EANN PES is compared with the corresponding DFT results in Figure 2, and the structural parameters of the stationary points along the reaction path are compared in Table 1. The agreement is generally quite good. These comparisons clearly suggest the high fidelity of the PES in representing the DFT data.

In Figure S1 of SI, the diffusion barriers for one O atom moving away from the other adsorbed O atom are shown for the  $9 \times 9$  model of the Ag(100) surface, which approaches the 0.68 eV value in the single O limit. Moreover, we calculated 2000 trajectories using the  $(3 \times 3)$ -Ag(100) model based on the EANN PES. The calculated dissociation probability of 5.6 % is consistent with the previous theoretical study by Alducin et al., <sup>61</sup> who reported a dissociation probability of ~5 % on a rigid  $(2 \times 2)$ -Ag(100) surface, under the same initial conditions of the incidence energy of 2.0 eV and normal incidence. Finally, we have compared the potential energy along an AIMD trajectory with that obtained on the PES in Figure S2. The agreement is quite satisfactory.

**Table 1.** Comparison of the structure parameters of potential minima and saddle points obtained from DFT and EANN PES. The center of mass height Z and internuclear distances between the two O atoms ( $d_{\text{O-O}}$ ), as well as the distance between an O atom and its nearest Ag atom ( $d_{\text{O-Ag}}$  (nm)), are listed. O1 and O2 represent the two oxygen atoms on the left and right of the center of mass in Figure 2, respectively.

Configuration	$Z_{\rm O1}$ (nm)	$Z_{O2}$ (nm)	$d_{ m O1 ext{-}Ag}$	$d_{ ext{O2-Ag}}( ext{nm})$	$d_{ ext{O-O}}$
			(nm)		(nm)
MIN1-DFT	0.160	0.160	0.233	0.233	0.143
MIN1-PES	0.159	0.159	0.233	0.233	0.143
SP1-DFT	0.139	0.139	0.211	0.211	0.237
SP1-PES	0.138	0.138	0.211	0.211	0.238
MIN2-DFT	0.070	0.070	0.221	0.221	0.326

MIN2-P	ES	0.069	0.069	0.221	0.221	0.325
SP2-DF	FT	0.138	0.072	0.208	0.228	0.451
SP2-PE	ES	0.139	0.073	0.208	0.228	0.451
MIN3-D	FT	0.070	0.070	0.221	0.221	0.326
MIN3-P	ES	0.069	0.069	0.221	0.221	0.325

#### IIIC. Dynamics of dissociation and diffusion

The dynamics of the dissociation and subsequent "hot" atom diffusion on the surface was simulated based on Newtonian mechanics. This is justified as the O atoms are quite heavy and free of significant quantum effects. Unlike the "hot" H atoms, <sup>20, 46</sup> the non-adiabatic coupling of O atoms with the surface electron-hole pairs is known to be quite weak. <sup>42, 64</sup> As a result, an adiabatic treatment of the dynamics is reasonable.

Energy dissipation from "hot" adsorbed species to surface phonons is challenging to simulate, because an accurate description of the surface phonons, especially for long wavelength ones, requires a very large supercell in a periodic model. 14, 16, 41, 42, 65 The periodicity on the surface might introduce further errors for diffusion. Therefore, we first discussed the influence of the supercell size on "hot" O atom diffusion on the Ag(100) surface, using a ten layer model with the surface size ranging from 3×3 to 15×15. This was made possible because of the EANN form of the PES, which has a radial cutoff of 6 Å. For each supercell size, 12000 QCT trajectories were propagated with an incidence angle of 45° and a larger incident energy of 4 eV to achieve reasonable statistics for O<sub>2</sub> dissociation. The impact region was set within the reduced triangle ABC, as shown in Figure 1. The O<sub>2</sub> dissociation probability was found to remain at ~38%, as shown in Table S2 of SI, independent of the cell size.

Unlike  $O_2$  dissociation, the effect of cell size on the diffusion of the "hot" atoms on the Ag(100) surface is not negligible. The averaged O-O distance of all trajectories is plotted as a function of time in the upper panel of Figure 3 for different cell sizes. (Note that in our calculations the corresponding supercell length is added to the O-O separation when one O passes through the cell boundary). It is clear from this plot that the initial separation of the two adsorbed atoms occurs immediately after the

dissociation, but the mobility drops to zero near 1.0 ps with an averaged separation of  $\sim$ 0.7 nm. The eventual convergence of the cell size is quite apparent. The lower panel of Figure 3 shows the distribution of the final O-O separation following O<sub>2</sub> dissociation for different cell sizes. It is clear that the distribution extends to 9 SLCs despite a prominent peak at 2 SLCs. When the O diffusion distance reaches 7 SLCs, close to 2 nm, the diffusion probability converges to the value of 0.6 % as the supercell size increases. We can see that the (3  $\times$  3) cell is definitely too small, but the (9  $\times$  9) cell is sufficient to describe the diffusion dynamics of the "hot" O atoms on Ag(100) as it is large enough to cover the diffusion of the "hot" O atoms without resorting to neighboring cells. However, the calculated O-O separation does not go beyond 2 nm, even with the unrealistically high incidence energy.

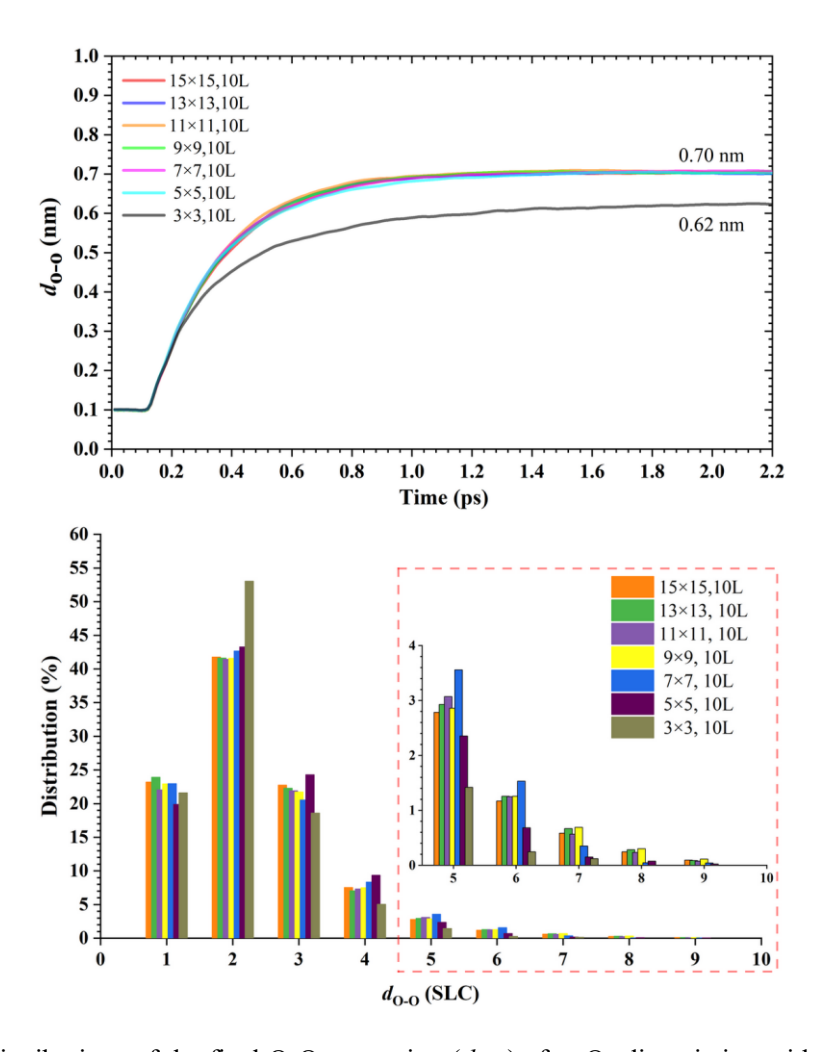


**Figure 3.** Distributions of the final O-O separation  $(d_{O-O})$  after  $O_2$  dissociation with different cell sizes. The impinging  $O_2(v_i = 0, j_i = 0)$  has an incidence angle of 45° and incidence energy of 4 eV.

Using the  $(9 \times 9)$  cell model, the calculated spatial distribution of the final position of the "hot" O atoms on the Ag(100) surface is shown in the left panel of Figure 4. Here the impact site is placed at the center of the cell (A in the figure). It is immediately clear from the figure that the diffusion of the "hot" O atoms on the Ag(100) surface is not isotropic and the diffusion along the X and Y directions is more facile than along other directions. This is also illustrated by the angular distribution in the right panel of the same figure, where two distinct peaks are observed. The diffusion anisotropy is dictated by the potential energy landscape, which favors the motion of O atoms along the X and Y directions despite the strong corrugation, as shown in Figure 5.

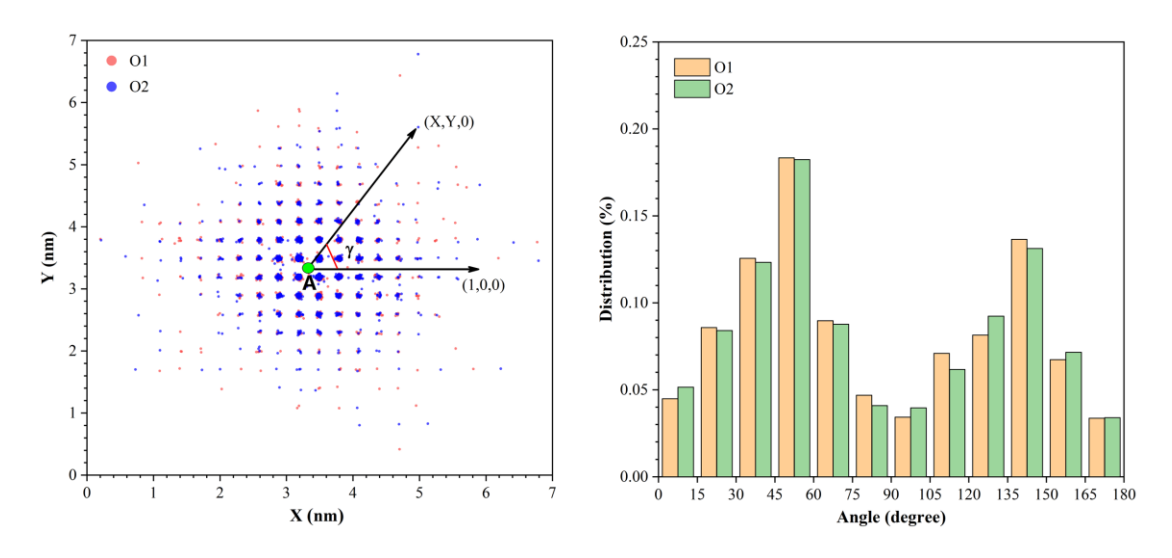


**Figure 4.** Left panel: Final positions of the two oxygen atoms (O1 and O2) after dissociation of O<sub>2</sub> on Ag(100). The impact region is within the reduced triangle ABC shown in Figure 1. This angle  $\gamma$  refers to the angle between the vector of an O atom relative to the A point and the (1,0,0) vector. Right panel: Final angular distributions of the two dissociated oxygen atoms using the 9×9 supercell.

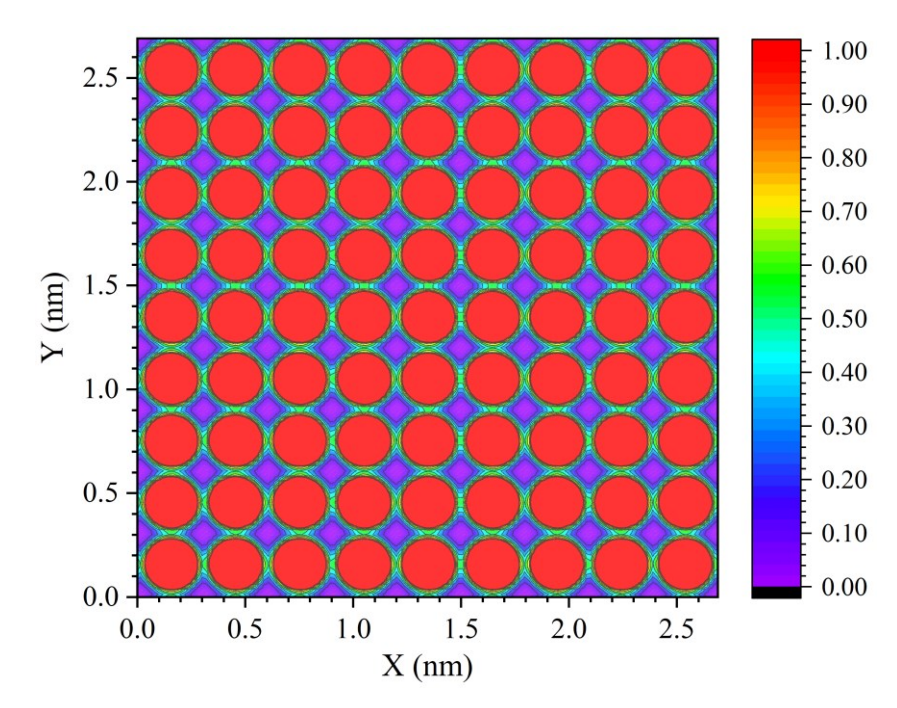


**Figure 5.** Diffusion potential energy landscape for a single atomic oxygen on the  $(3\times3)$  Ag(100) surface at Z = 0.134 nm, which corresponds to the diffusion transition state.

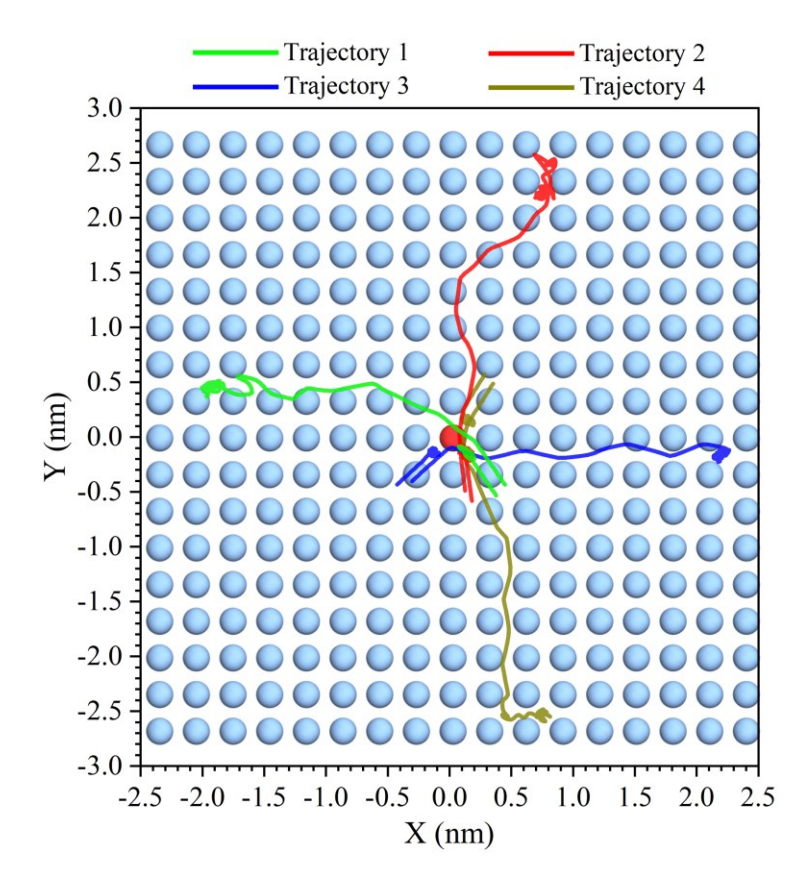


**Figure 6.** A few exemplary trajectories of the two dissociated oxygen atoms with large final O-O separations. For clarity, only the top view of the surface is shown. The red sphere represents the Ag atom closest to the impact site.

A few exemplary trajectories undergoing far-ranged diffusion are shown in Figure 6. Similar to previous observations for  $H_2^{13, 20, 46}$  and  $N_2$  dissociation,<sup>21</sup> only one of the two O atoms typically travels a long distance while the other remains trapped after dissociation. After dissociation, the O atom migrates over a considerable distance within ~1 ps before getting trapped at a hollow site. As expected, the migration of the roaming O atom is mostly along the *X* or *Y* direction, facilitated by the low-energy diffusion channels provided by the PES, as shown in Figure 5.

It is interesting to examine the far-ranged diffusion of the O atom in these exemplary trajectories. In Figure 7, we plot the four exemplary trajectories in Z and d, which is the distance between the O atom and the impact site. It is quite clear that one of the two O atoms is trapped near the impact site and its fluctuation in Z is seldom above 0.15 nm, which is slightly higher than the Z value of the diffusion barrier (0.139 nm). On the other hand, the other O atom undergoes fast diffusion, with Z typically above 0.15 nm and rarely trapped in the potential well at the hollow site until the end. Movies of these trajectories can be found in SI.

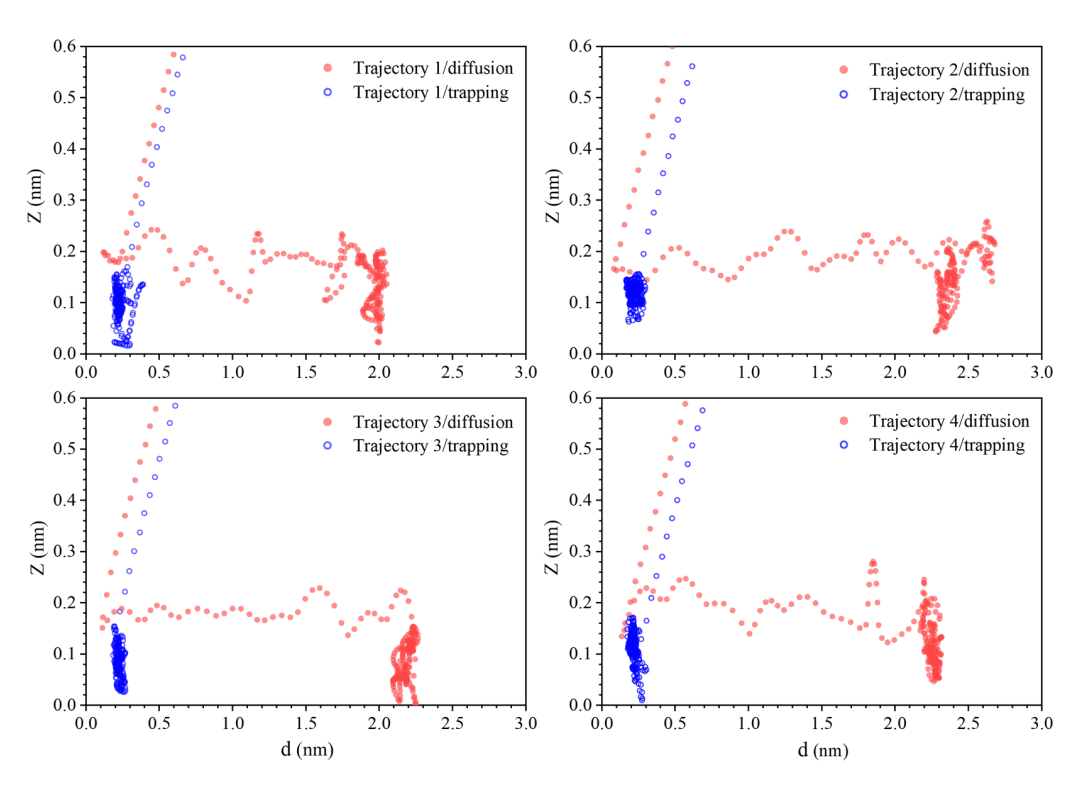


**Figure 7.** Evolution of the O atoms described by their height above the surface (Z) and distance from the impact site (d).

The final O-O separation depends on the initial conditions of the impinging O<sub>2</sub> molecule. As shown in Figure 8, the reduction of the incidence energy to 2 eV significantly reduces the final O-O separation, with a distribution peaking at 1 SLC. Vibrational excitation of the impinging O<sub>2</sub> molecule to  $v_i = 2$  or rotational excitation to  $j_i = 2$  seem to have a relatively limited impact on the distribution. On the other hand, the change of the incidence angle from the surface normal to  $\theta_i = 45^{\circ}$  increases the final O-O separation.

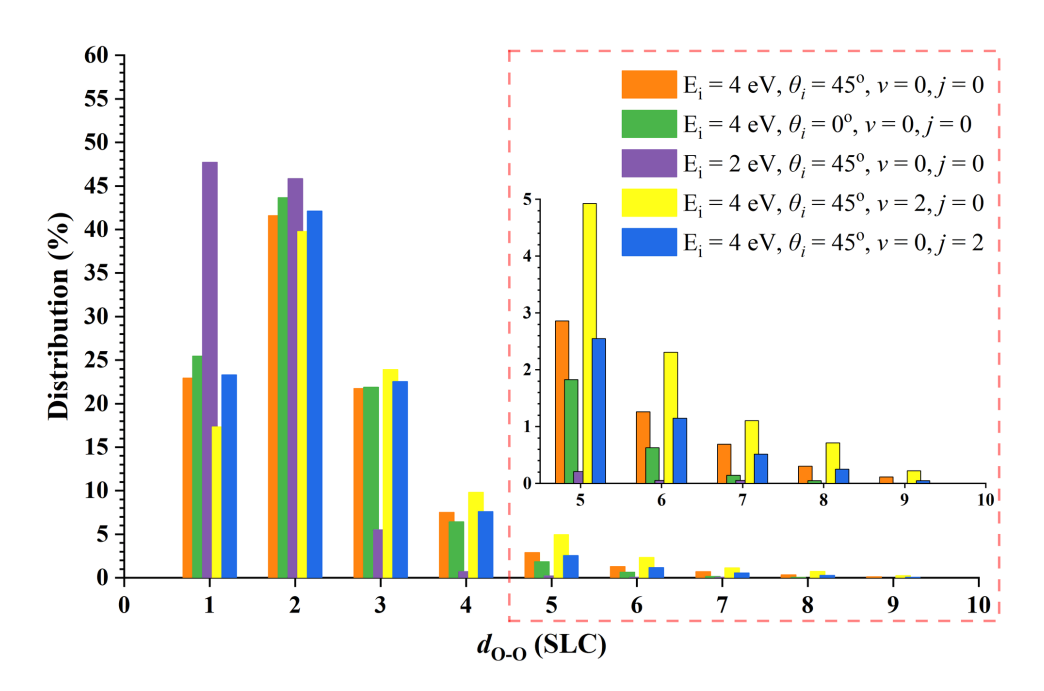


**Figure 8.** Distributions of the O-O separation ( $d_{\text{O-O}}$ ) after O<sub>2</sub> dissociation with different initial conditions.

The calculation results presented so far are all with high incidence energies, which allowed us to have a sufficient number of dissociation events for studying the subsequent "hot" O dynamics. However, the STM experiments of Morgenstern and coworkers<sup>31, 34</sup> used ambient O<sub>2</sub> to prepare the O atoms on Ag(100). Because of the relatively high dissociation barrier for O<sub>2</sub> on Ag(100), the dissociation probability at the experimental temperatures is quite low and difficult to simulate, we elected to prepare the nascent "hot" O atoms using a different strategy.

For the post-dissociation dynamics at low temperatures, where the impinging O<sub>2</sub> is likely to first molecularly adsorb on the Ag(100) surface, the overcoming of the dissociation barrier is expected to be thermally driven. Hence, the kinetic energy of the two O atoms originates from the energy release from O<sub>2</sub> dissociation. In our simulation, the O<sub>2</sub> molecule was placed at the dissociation transition state (SP1) above the hollow site of the surface at 0 K. The initial velocities of the two O atoms were randomly assigned with a negligible kinetic energy of 50 meV.

2800 trajectories were propagated using the 9×9 model of the Ag(100) surface. As shown in Figure 9, the distribution of the final O-O separation ( $d_{\text{O-O}}$ ) is dominated by the population at 2 SLCs (0.6 nm), with the maximum  $d_{\text{O-O}}$  at 3 SLCs with an extremely low probability of 0.3 %. This distance is about an order of magnitude shorter than the experimental distribution derived from STM measurements (2 and 4 nm).<sup>34</sup> Furthermore, diffusion only occurs along the X or Y direction of the surface.

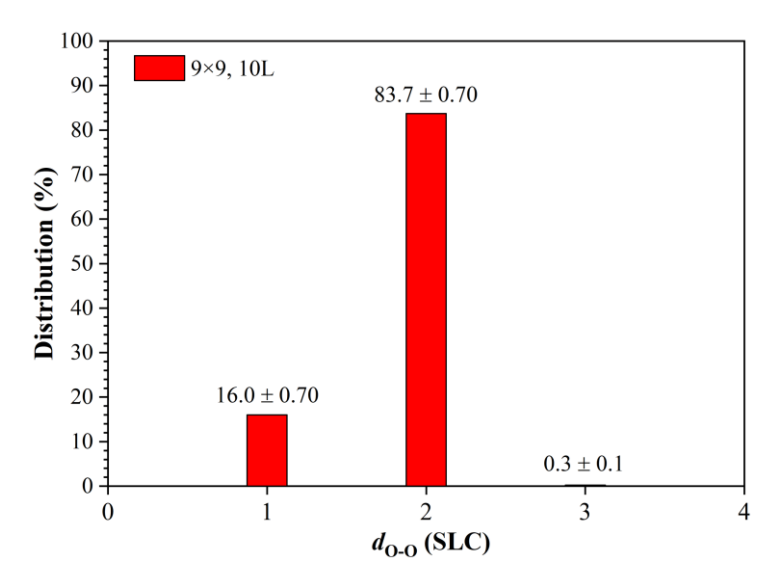


**Figure 9.** Distribution of the O-O separation ( $d_{O-O}$ ), starting at the O<sub>2</sub> dissociation transition state.

To understand the observed dynamics, Figure 10 shows the total kinetic energy of the Ag atoms and the atomic oxygen adsorbates. The components of the kinetic energy of the two O atoms along the X, Y, and Z directions are also shown along with the O-O separation ( $d_{O-O}$ ) and the corresponding X, Y, and Z coordinates of the two O

atoms as a function of time for an exemplary trajectory. As the O<sub>2</sub> dissociates from the TS, the O1 and O2 atoms reach the bottom of the adsorption wells at the time of 140 and 200 fs, respectively, with maximum kinetic energies of ~0.9 and ~0.6 eV parallel to the surface. This is expected as the total energy release from the dissociation is about 1.8 eV, which is disposed into the two O atoms. However, their kinetic energies quickly dissipate into the surface photons, as evidenced by the rise of the Ag kinetic energy, such that they become less than the diffusion barrier (0.68 eV) and no ballistic diffusion was observed beyond the 2 SCL separation (0.6 nm). After 800 fs, the energy dissipation rate levels off, accompanied by greatly reduced kinetic energy of oxygen atoms, making further diffusion of oxygen atoms unlikely.

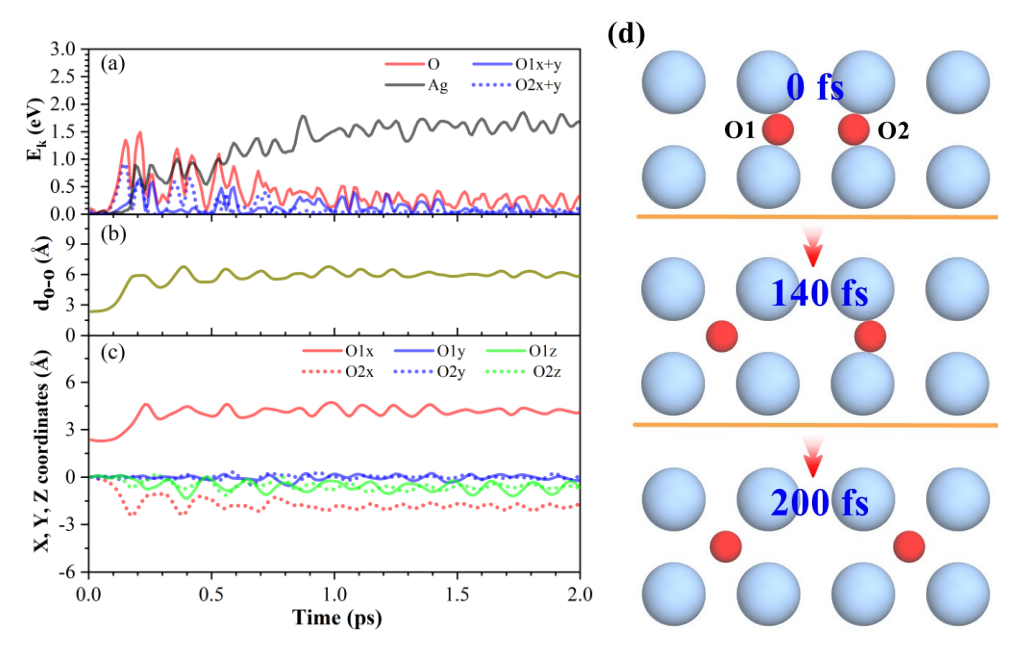


**Figure 10.** Evolution of an exemplary trajectory. (a) total kinetic energies of the Ag atoms and atomic oxygen adsorbates, as well as O components parallel (X + Y) to the surface, (b) distance between oxygen atoms  $(d_{O-O})$ , (c) the corresponding X, Y, and Z coordinates of the two O atoms and (d) snapshots of O diffusion on the  $(9\times9\times10 \text{ L})$  Ag(100) slab as a function of time for an exemplary trajectory ending at the  $d_{O-O} = 2$  SLCs.

# **IV. Discussion**

There is a long-held view in the field about the "hot" atom dynamics on surfaces

that such atoms produced by dissociative chemisorption might travel long distances before equilibration. Indeed, discussions in the literature have invoked such a scenario to rationalize surface reactions.<sup>3,4</sup> Unfortunately, much of the evidence has so far been from STM, which is based on static measurements of the equilibrated distribution of adsorbed atoms. Recently, there is increasing evidence questioning the conclusion that the observed large pair distances can indeed be attributed to high mobility of "hot" atoms on metal surfaces. Experimentally, Schmid et al.,<sup>32</sup> have presented evidence disputing the earlier STM data of Brune et al.<sup>26, 27</sup> for the large O-O distances (>8 nm) on Al(111). Theoretically, several recent state-of-the-art studies based on machine learned first principles PESs have been unable to reproduce some previous STM observations of "hot" atom migration beyond 1 nm on metal surfaces.<sup>21, 42</sup> The validation of this long-held belief, the elucidation of its origin, and the quantitative determination of the extent of "hot" atom surface dynamics are thus of great importance for a better understanding of "hot" atom induced chemistry.

The significantly shorter O-O separation from our thermal simulations on Ag(100) than the STM values is reminiscent of the recent theory-experiment disagreement in the "hot" N diffusion after N<sub>2</sub> dissociation on Ru(0001). 11, 21 Our calculated final N-N separation<sup>21</sup> is about one order of magnitude smaller than the STM results (~7 nm). 11 The diffusion barrier for N on Ru(0001) of 0.86 eV is comparable with that for O on Ag(100), namely 0.68 eV. As a result, it is not surprising that the diffusion lengths of the "hot" atoms are comparable. We further note that the most recent first-principles study of "hot" O atom dynamics upon O<sub>2</sub> dissociation on Pd surfaces has also yielded relatively short (< 1 nm) O-O separations, 42 in agreement with STM results. 33 In particular, the previously reported observation of high transient mobility of "hot" O atoms on Pd(100)<sup>14</sup> was found to be a rare event. 42 While our DFT results do indicate repulsive interactions between adjacent O atoms, this interaction is rather short ranged and insufficient to reproduce the observed large O-O separations.

There are many possible reasons for the theory-experiment discrepancies. Theoretically, it is possible that the DFT characterization of the electronic structure is not sufficiently accurate. There is well known that the barrier determined by DFT may depend on the functional used in the calculation. For the current system, we have calculated the diffusion barrier using several GGA functionals, as discussed in SI (Table S1), and no significant difference was found.

It has been argued that the far-ranged O motion could be the result of the so-called "cannonball" process,<sup>7, 66</sup> in which one of the two O atoms undergoes "frustrated" desorption as the other become chemisorbed. We have not observed any trajectories with such characteristics. This is readily understood that the O atom adsorbs strongly on the Ag surface and the dissociation transition state features an O<sub>2</sub> species parallel to the surface plane.

We note that the O<sub>2</sub> molecule exists in the gas phase as a triplet species, and it might undergo spin flip to become a singlet species as it approaches the surface, which might change the dynamics. A similar proposal was invoked to explain the activated nature of O<sub>2</sub> dissociation on Al(111).<sup>67</sup> However, later theoretical calculations dismissed this hypothesis and attributed the lack of an activation barrier in DFT calculations to the self-interaction error.<sup>68</sup> Dynamical calculations based on an embedded wavefunction PES reproduced the experimental data,<sup>69</sup> without considering the triplet-singlet curve crossing. For the system investigated here, we have carried out DFT calculations on the adsorption and diffusion of atomic oxygen on Ag(100), assuming zero and two unpaired electrons, which correspond to the singlet and triplet states. The results in Table S3 show very minor differences, which suggest an insignificant role played by the electronic spin of the O<sub>2</sub> molecule.

On the other hand, it is important to point out that STM is not a direct method for following the ballistic dynamics, which is inferred from the equilibrated spatial distribution of the atoms. It is difficult to assign the O pairs in the STM image to the original O<sub>2</sub> molecule and a statistical analysis was needed to obtain the distribution.<sup>31, 34</sup> In addition, we note that in another low-temperature STM study, where the adsorbed O<sub>2</sub> is dissociated by inelastic electron tunneling, the O-O separation is only 1-2 nm,<sup>43</sup> smaller than the thermal dissociation. However, this situation is markedly different from the thermal case. In addition, thermal diffusion, which takes a much

longer time than our simulations could cover, cannot be completely ruled out due to the finite temperature. Due to the relatively short simulation time, thermal diffusion is not included in our model. It appears that the STM observations might be the result of yet unknown mechanisms that are not included in our theoretical model. A definitive elucidation of the post-dissociation dynamics of "hot" O atoms on metal surfaces would require further experimental and theoretical explorations.

Finally, it is interesting to compare the "hot" atom dynamics discussed in this work with the so-called "precursor-mediated mechanism" that involves molecular species.<sup>1</sup> In the latter case, molecules trapped on a solid surface, namely the "precursor", often undergoes significant ballistic motion before reaction. <sup>17-19, 70-72</sup> The key difference is that molecular adsorbates are typically trapped in a physisorbed well typically with a low diffusion barrier, while atomic species often chemisorb on metal surfaces that have significant diffusion barriers. The surface corrugation in the latter case tends to lead to much more efficient energy dissipation to surface phonons.

# V. Conclusions

In this work, we took advantage of machine learning to develop a first-principles based high-dimensional PES which is capable of describing the O/O<sub>2</sub> interaction with the Ag(100) surface with different supercell sizes. The PES allowed us to examine the influence of the cell size on the dynamics of "hot" O atoms on Ag(100) upon dissociative chemisorption. These translationally "hot" atomic adsorbates acquire significant translational energies through the exothermic dissociation process, leading to mobility along the surface. However, these "hot" species are also subjected to energy dissipation to surface phonons. Our simulations found a strong anisotropy in the early dynamics of the "hot" O atoms, due apparently to the angular dependence of the surface corrugation. These results also suggest that the large O-O separations over 1 nm can only be achieved with hyperthermal impinging O<sub>2</sub>, while its thermal dissociation results in sub-nanometer separations. The relatively short O migration despite the imparting energy from the dissociation of O<sub>2</sub> suggests relatively efficient

energy dissipation to the surface, which prevents the O atoms from overcoming the significant diffusion barrier. The emergence of accurate first-principles based simulations raises questions about the origin(s) of the experimentally reported farranged O diffusion in the current and other systems, and further investigations are needed to resolve the theory-experiment inconsistencies.

Acknowledgements: This work was supported by US National Science Foundation (Grant Nos. CHE-1951328 and CHE-2306975 to H. G.), National Natural Science Foundation of China (Grant No. 21973013 to S. L.) and the National Natural Science Foundation of Fujian Province, China (Grant No. 2020J02025 to S. L.), and the "Chuying Program" for the Top Young Talents of Fujian Province. The computation was performed at the Hefei Advanced Computing Center and Supercomputing Center of Fujian and at the Center for Advanced Research Computing (CARC) at UNM. We thank Prof. Bin Jiang for sharing his work (Ref. <sup>42</sup>) prior to publication and for many stimulating discussions and Prof. Karina Morgenstern for useful discussions.

**Supporting Information**: Additional results including the diffusion barrier, convergence of the PES, functional dependence of the diffusion barrier for atomic oxygen on Ag(100), size dependence of the dissociation probability, effect of spin, four movies for "hot" O dynamics, and the Fortran code for the PES (including seven files and readme).

#### REFERENCES

- (1) Harris, J.; Kasemo, B. On precursor mechanims for surface reactions. *Surf. Sci.* **1981**, *105*, L281-L287.
- (2) Carley, A. F.; Davies, P. R.; Roberts, M. W. The development of a new concept: The role of oxygen transients, defect and precursor states in surface reactions. *Catal. Lett.* **2002**, *80*, 25-34.
- (3) Mieher, W. D.; Ho, W. Photochemistry of oriented molecules coadsorbed on solid surfaces: The formation of CO<sub>2</sub>+O from photodissociation of O<sub>2</sub> coadsorbed with CO on Pt(111). *J. Chem. Phys.* **1989**, *91*, 2755-2756.
- (4) Kyriakou, G.; Boucher, M. B.; Jewell, A. D.; Lewis, E. A.; Lawton, T. J.; Baber, A. E.; Tierney, H. L.; Flytzani-Stephanopoulos, M.; Sykes, E. C. H. Isolated metal atom geometries as a strategy for selective heterogeneous hydrogenations. *Science* **2012**, *335*, 1209.
- (5) Alducin, M.; Díez Muiño, R.; Juaristi, J. I. Non-adiabatic effects in elementary reaction processes at metal surfaces. *Prog. Surf. Sci.* **2017**, *92*, 317-340.
- (6) Rittmeyer, S. P.; Bukas, V. J.; Reuter, K. Energy dissipation at metal surfaces. *Adv. Phys. X* **2018**, *3*, 1381574.
- (7) Diebold, U.; Hebenstreit, W.; Leonardelli, G.; Schmid, M.; Varga, P. High transient mobility of chlorine on TiO<sub>2</sub>(110): Evidence for "cannon-ball" trajectories of hot adsorbates. *Phys. Rev. Lett.* **1998**, *81*, 405-408.
- (8) Jewell, A. D.; Peng, G.; Mattera, M. F. G.; Lewis, E. A.; Murphy, C. J.; Kyriakou, G.; Mavrikakis, M.; Sykes, E. C. H. Quantum tunneling enabled self-assembly of hydrogen atoms on Cu(111). *ACS Nano* **2012**, *6*, 10115-10121.
- (9) Dombrowski, E.; Peterson, E.; Del Sesto, D.; Utz, A. L. Precursor-mediated reactivity of vibrationally hot molecules: Methane activation on Ir(111). *Catal. Today* **2015**, *244*, 10-18.
- (10) Shirhatti, P. R.; Rahinov, I.; Golibrzuch, K.; Werdecker, J.; Geweke, J.; Altschäffel, J.; Kumar, S.; Auerbach, D. J.; Bartels, C.; Wodtke, A. M. Observation of the adsorption and desorption of vibrationally excited molecules on a metal surface. *Nat. Chem.* **2018**, *10*, 592-598.
- (11) Wagner, J.; Grabnic, T.; Sibener, S. J. STM visualization of N<sub>2</sub> dissociative chemisorption on Ru(0001) at high impinging kinetic energies. *J. Phys. Chem. C* **2022**, *126*, 18333-18342.
- (12) Sitz, G. O.; Mullins, C. B. Molecular dynamics simulations of the influence of surface temperature on the trapping of methane on iridium single-crystalline surfaces. *J. Phys. Chem. B* **2002**, *106*, 8349-8353.
- (13) Ramos, M.; Martínez, A. E.; Busnengo, H. F. H<sub>2</sub> dissociation on individual Pd atoms deposited on Cu(111). *Phys. Chem. Chem. Phys.* **2012**, *14*, 303-310.
- (14) Meyer, J.; Reuter, K. Modeling heat dissipation at the nanoscale: an embedding approach for chemical reaction dynamics on metal surfaces. *Angew. Chem. Int. Ed.* **2014**, *53*, 4721-4724.
- (15) Guo, S. Y.; Jenkins, S. J.; Ji, W.; Ning, Z.; Polanyi, J. C.; Sacchi, M.; Wang, C.-G. Repulsion-induced surface-migration by ballistics and bounce. *J. Phys. Chem. Lett.* **2015**, *6*, 4093-4098.

- (16) Bukas, V. J.; Reuter, K. Hot adatom diffusion following oxygen dissociation on Pd(100) and Pd(111): A first-principles study of the equilibration dynamics of exothermic surface reactions. *Phys. Rev. Lett.* **2016**, *117*, 146101.
- (17) Huang, M.; Zhou, X.; Zhang, Y.; Zhou, L.; Alducin, M.; Jiang, B.; Guo, H. Adiabatic and nonadiabatic energy dissipation during scattering of vibrationally excited CO from Au(111). *Phys. Rev. B* **2019**, *100*, 201407(R).
- (18) Moiraghi, R.; Lozano, A.; Peterson, E.; Utz, A.; Dong, W.; Busnengo, H. F. Nonthermalized precursor-mediated dissociative chemisorption at high catalysis temperatures. *J. Phys. Chem. Lett.* **2020**, *11*, 2211-2218.
- (19) Zhou, X.; Zhang, Y.; Guo, H.; Jiang, B. Towards bridging the structure gap in heterogeneous catalysis: the impact of defects in dissociative chemisorption of methane on Ir surfaces. *Phys. Chem. Chem. Phys.* **2021**, *23*, 4376-4385.
- (20) Gu, K.; Wei, F.; Cai, Y.; Lin, S.; Guo, H. Dynamics of initial hydrogen spillover from a single atom platinum active site to the Cu(111) host surface: The impact of substrate electron–hole pairs. *J. Phys. Chem. Lett.* **2021**, *12*, 8423-8429.
- (21) Wang, Y.; Guo, H. Post-dissociation dynamics of N<sub>2</sub> on Ru(0001): How far can the "Hot" N atoms travel? *J. Phys. Chem. C* **2023**, *127*, 4079-4086.
- (22) Andersen, M.; Panosetti, C.; Reuter, K. A practical guide to surface kinetic Monte Carlo simulations. *Front. Chem.* **2019**, *7*.
- (23) Bruix, A.; Margraf, J. T.; Andersen, M.; Reuter, K. First-principles-based multiscale modelling of heterogeneous catalysis. *Nat. Catal.* **2019**, *2*, 659-670.
- (24) Montemore, M. M.; van Spronsen, M. A.; Madix, R. J.; Friend, C. M. O<sub>2</sub> activation by metal surfaces: Implications for bonding and reactivity on heterogeneous catalysts. *Chem. Rev.* **2018**, *118*, 2816-2862.
- (25) Nolan, P. D.; Wheeler, M. C.; Davis, J. E.; Mullins, C. B. Mechanisms of initial dissociative chemisorption of oxygen on transition-metal surfaces. *Acc. Chem. Res.* **1998**, *31*, 798-804.
- (26) Brune, H.; Wintterlin, J.; Behm, R. J.; Ertl, G. Surface migration of "hot" adatoms in the course of dissociative chemisorption of oxygen on Al(111). *Phys. Rev. Lett.* **1992**, *68*, 624-626.
- (27) Brune, H.; Wintterlin, J.; Trost, J.; Ertl, G.; Wiechers, J.; Behm, R. J. Interaction of oxygen with Al(111) studied by scanning tunneling microscopy. *J. Chem. Phys.* **1993**, *99*, 2128-2148.
- (28) Wintterlin, J.; Schuster, R.; Ertl, G. Existence of a "hot" atom mechanism for the dissociation of O<sub>2</sub> on Pt(111). *Phys. Rev. Lett.* **1996**, 77, 123-126.
- (29) Briner, B. G.; Doering, M.; Rust, H. P.; Bradshaw, A. M. Mobility and trapping of molecules during oxygen adsorption on Cu(110). *Phys. Rev. Lett.* **1997**, *78*, 1516-1519.
- (30) Hla, S. W.; Lacovig, P.; Comelli, G.; Baraldi, A.; Kiskinova, M.; Rosei, R. Orientational anisotropy in oxygen dissociation on Rh(110). *Phys. Rev. B* **1999**, *60*, 7800-7803.
- (31) Schintke, S.; Messerli, S.; Morgenstern, K.; Nieminen, J.; Schneider, W.-D. Farranged transient motion of "hot" oxygen atoms upon dissociation. *J. Chem. Phys.* **2001**, *114*, 4206-4209.

- (32) Schmid, M.; Leonardelli, G.; Tscheließnig, R.; Biedermann, A.; Varga, P. Oxygen adsorption on Al(111): low transient mobility. *Surf. Sci.* **2001**, *478*, L355-L362.
- (33) Rose, M. K.; Borg, A.; Dunphy, J. C.; Mitsui, T.; Ogletree, D. F.; Salmeron, M. Chemisorption of atomic oxygen on Pd(111) studied by STM. *Surf. Sci.* **2004**, *561*, 69-78.
- (34) Hsieh, M.-F.; Lin, D.-S.; Gawronski, H.; Morgenstern, K. Hard repulsive barrier in hot adatom motion during dissociative adsorption of oxygen on Ag(100). *J. Chem. Phys.* **2009**, *131*, 174709.
- (35) Klobas, E. J.; Schmid, M.; Friend, C. M.; Madix, R. J. The dissociation-induced displacement of chemisorbed O<sub>2</sub> by mobile O atoms and the autocatalytic recombination of O due to chain fragmentation on Ag(110). *Surf. Sci.* **2014**, *630*, 187-194.
- (36) Wahnström, G.; Lee, A. B.; Strömquist, J. Motion of "hot" oxygen adatoms on corrugated metal surfaces. *J. Chem. Phys.* **1996**, *105*, 326-336.
- (37) Ciacchi, L. C.; Payne, M. C. "Hot-Atom" O<sub>2</sub> dissociation and oxide nucleation on Al(111). *Phys. Rev. Lett.* **2004**, *92*, 176104.
- (38) Perron, N.; Pineau, N.; Arquis, E.; Rayez, J. C.; Salin, A. Adsorption of atomic oxygen on the Cu(100) surface. *Surf. Sci.* **2005**, *599*, 160-172.
- (39) Sendner, C.; Groß, A. Kinetic Monte Carlo simulations of the interaction of oxygen with Pt(111). *J. Chem. Phys.* **2007**, *127*, 014704.
- (40) Groß, A. Ab initio molecular dynamics study of hot atom dynamics after dissociative adsorption of H<sub>2</sub> on Pd(100). *Phys. Rev. Lett.* **2009**, *103*, 246101.
- (41) Bukas, V. J.; Reuter, K. Phononic dissipation during "hot" adatom motion: A QM/Me study of O<sub>2</sub> dissociation at Pd surfaces. *J. Chem. Phys.* **2017**, *146*, 014702.
- (42) Lin, Q.; Jiang, B. First-principles mdeling of equilibration dynamics of hyperthermal products of surface reactions using scalable neural network potential. *J. Phys. Chem. Lett.* **2023**, *14*, 7513–7518.
- (43) Sprodowski, C.; Mehlhorn, M.; Morgenstern, K. Dissociation of oxygen on Ag(100) induced by inelastic electron tunneling. *J. Phys. Condens. Mat.* **2010**, *22*, 264005.
- (44) Behler, J. First principles neural network potentials for reactive simulations of large molecular and condensed systems. *Angew. Chem. Int. Ed.* **2017**, *56*, 12828-12840.
- (45) Jiang, B.; Li, J.; Guo, H. High-fidelity potential energy surfaces for gas phase and gas-surface scattering processes from machine learning. *J. Phys. Chem. Lett.* **2020**, *11*, 5120-5131.
- (46) Gu, K.; Li, C.; Jiang, B.; Lin, S.; Guo, H. Short- and long-time dynamics of hydrogen spillover from a single atom platinum active site to the Cu(111) host surface. *J. Phys. Chem. C* **2022**, *126*, 17093-17101.
- (47) Kresse, G.; Furthmuller, J. Efficient iterative schemes for ab initio total-energy calculations using plane wave basis set. *Phys. Rev. B* **1996**, *54*, 11169-11186.
- (48) Kresse, G.; Furthmuller, J. Efficiency of ab initio total energy calculations for metals and semiconductors using plane wave basis set. *Comp. Mater. Sci.* **1996**, *6*, 15-50.

- (49) Blöchl, P. E. Projector augmented-wave method. *Phys. Rev. B* **1994**, *50*, 17953-17979.
- (50) Hammer, B.; Hansen, L. B.; Nørskov, J. K. Improved adsorption energetics within density functional theory using revised Perdew-Burke-Ernzerhof functionals. *Phys. Rev. B* **1999**, *59*, 7413-7421.
- (51) Henkelman, G.; Uberuaga, B. P.; Jónsson, H. A climbing image nudged elastic band method for finding saddle points and minimum energy paths. *J. Chem. Phys.* **2000**, *113*, 9901-9904.
- (52) Zhang, Y.; Hu, C.; Jiang, B. Embedded atom neural network potentials: Efficient and accurate machine learning with a physically inspired representation. *J. Phys. Chem. Lett.* **2019**, *10*, 4962-4967.
- (53) Behler, J.; Parrinello, M. Generalized neural-network representation of high-dimensional potential-energy surfaces. *Phys. Rev. Lett.* **2007**, *98*, 146401.
- (54) Lin, Q.; Zhang, Y.; Zhao, B.; Jiang, B. Automatically growing global reactive neural network potential energy surfaces: A trajectory-free active learning strategy. *J. Chem. Phys.* **2020**, *152*, 154104.
- (55) Lin, Q.; Zhang, L.; Zhang, Y.; Jiang, B. Searching configurations in uncertainty space: Active learning of high-dimensional neural network reactive potentials. *J. Chem. Theo. Comput.* **2021**, *17*, 2691-2701.
- (56) Jiang, B.; Guo, H. Dynamics of water dissociative chemisorption on Ni(111): Effects of impact sites and incident angles. *Phys. Rev. Lett.* **2015**, *114*, 166101.
- (57) Hase, W. L.; Duchovic, R. J.; Hu, X.; Komornicki, A.; Lim, K. F.; Lu, D.-H.; Peslherbe, G. H.; Swamy, K. N.; Linde, S. R. V.; Varandas, A.; et al. VENUS96: A General Chemical Dynamics Computer Program. *Quantum Chemistry Program Exchange Bulletin* **1996**, *16*, 671.
- (58) Software Library of the Computer Center for Institute for Molecular Science.
- (59) Vattuone, L.; Gambardella, P.; Valbusa, U.; Rocca, M. HREELS study of O<sub>2</sub> molecular chemisorption on Ag(001). *Surf. Sci.* **1997**, *377-379*, 671-675.
- (60) Buatier de Mongeot, F.; Rocca, M.; Cupolillo, A.; Valbusa, U.; Kreuzer, H. J.; Payne, S. H. Sticking and thermal desorption of O<sub>2</sub> on Ag(001). *J. Chem. Phys.* **1997**, *106*, 711-718.
- (61) Alducin, M.; Busnengo, H. F.; Muiño, R. D. Dissociative dynamics of spin-triplet and spin-singlet O<sub>2</sub> on Ag(100). *J. Chem. Phys.* **2008**, *129*, 224702.
- (62) Gajdoš, M.; Eichler, A.; Hafner, J. Ab initio density functional study of O on the Ag(001) surface. *Surf. Sci.* **2003**, *531*, 272-286.
- (63) Wang, Y.; Jia, L.; Dai, W.; Wang, W.; Fan, K. Theoretical study about adsorption of atomic oxygen on unmodified and I-modified Ag(100) surface. *J. Chem. Phys.* **2003**, *118*, 11210-11216.
- (64) Meyer, J.; Reuter, K. Electron-hole pairs during the adsorption dynamics of O<sub>2</sub> on Pd(100): exciting or not? *New J. Phys.* **2011**, *13*, 085010.
- (65) Hu, C.; Lin, Q.; Jiang, B.; Guo, H. Influence of supercell size on gas-surface scattering: A case study of CO scattering from Au(111). *Chem. Phys.* **2022**, *554*, 111423.
- (66) Komrowski, A. J.; Sexton, J. Z.; Kummel, A. C.; Binetti, M.; Weiße, O.;

- Hasselbrink, E. Oxygen abstraction from dioxygen on the Al(111) surface. *Phys. Rev. Lett.* **2001**, *87*, 246103.
- (67) Behler, J.; Delley, B.; Lorenz, S.; Reuter, K.; Scheffler, M. Dissociation of O<sub>2</sub> at Al(111): The role of spin selection rules. *Phys. Rev. Lett.* **2005**, *94*, 036104.
- (68) Libisch, F.; Huang, C.; Liao, P.; Pavone, M.; Carter, E. A. Origin of the energy barrier to chemical reactions of O<sub>2</sub> on Al(111): Evidence for charge transfer, not spin selection. *Phys. Rev. Lett.* **2012**, *109*, 198303.
- (69) Yin, R.; Zhang, Y.; Libisch, F.; Carter, E. A.; Guo, H.; Jiang, B. Dissociative chemisorption of O<sub>2</sub> on Al(111): Dynamics on a correlated wave-function-based potential energy surface. *J. Phys. Chem. Lett.* **2018**, *9*, 3271-3277.
- (70) Seets, D. C.; Wheeler, M. C.; Mullins, C. B. Trapping-mediated and direct dissociative chemisorption of methane on Ir(110): A comparison of molecular beam and bulb experiments. *J. Chem. Phys.* **1997**, *107*, 3986-3998.
- (71) Zhou, X.; Jiang, B.; Guo, H. Dissociative chemisorption of methane on stepped Ir(332) surface: Density functional theory and ab initio molecular dynamics studies. *J. Phys. Chem. C* **2019**, *123*, 20893-20902.
- (72) Peludhero, I. F.; Gutiérrez-González, A.; Dong, W.; Beck, R. D.; Busnengo, H. F. Dissociative sticking probability of methane on Pt(110)-(2×1). *J. Phys. Chem. C* **2021**, *125*, 11904-11915.

# TOC graphic

